Materials and Structures (2024) 57:57
https://doi.org/10.1617/s11527-024-02336-8

ORIGINAL ARTICLE

Verification of the improved constitutive tensile model for fibre reinforced concrete

Brecht Vandevyvere · Lucie Vandewalle · Rutger Vrijdaghs · Hans Pauwels · Jiabin Li

Received: 17 January 2023 / Accepted: 11 March 2024 / Published online: 9 April 2024

Abstract Recently, new constitutive tensile models for describing the post-cracking behaviour of fibre reinforced concrete for different performance classes were developed by the author(s). The models are based on test data on notched beams with macro fibres, including one type of glass fibres and two polypropylene fibres. Nowadays, a wide range of macro fibres for reinforcing concrete mixtures is available. The objective of this paper is thus to examine whether the newly developed models are applicable for other FRC mixtures. For this purpose, the experimental results of 236 three-point bending tests on notched beams, obtained from Vrijdaghs et al. and the international company Bekaert, are compared with the model predictions. The results indicate that the proposed model for performance class *a* & *b* and class *c* exhibit a higher accuracy at $CMOD_1$ than the model in MC10 and EC2 (next version). However, further optimization is required at $CMOD_3$ for the model of performance class *a* & *b* and class *d*. A strong correlation is also found between the experimental f_{R1}-values, as well as the f_{R3}-values, and the predicted compression zone height of the beam cross-section at midspan by use of those new constitutive models. Moreover, this paper also proposes a modification to the model of Oettel et al. for better estimating the residual flexural tensile strength of FRC mixtures with 4D Dramix fibres.

Keywords Fibre reinforced concrete · Macro fibres · Constitutive tensile model · Post-cracking behaviour · Residual flexural tensile strength · Model verification

Rutger Vrijdaghs and Hans Pauwels have contributed equally to this work.

B. Vandevyvere (✉) · J. Li (✉)
Department of Civil Engineering, KU Leuven Campus Brugge, Spoorwegstraat 12, 8200 Brugge, Belgium
e-mail: brecht.vandevyvere@kuleuven.be

J. Li
e-mail: jiabin.li@kuleuven.be

L. Vandewalle
Department of Civil Engineering, KU Leuven, Kasteelpark Arenberg 40, 3001 Louvain, Belgium
e-mail: lucie.vandewalle@kuleuven.be

R. Vrijdaghs
Laboratory Structures and Building Systems, Buildwise, Avenue Pierre Holoffe 21, 1342 Limelette, Belgium
e-mail: rutger.vrijdaghs@buildwise.be

H. Pauwels
Concrete Expertise Center, NV Bekaert SA, Oude Heerweg 5, 8540 Deerlijk, Belgium
e-mail: Hans.Pauwels@bekaert.com

1 Introduction

Fibre reinforced concrete (FRC) is a composite material in which randomly distributed and oriented fibres are added to the concrete mixture. The bridging effect of the fibres results in an improved tensile cracking capacity that significantly enhances the low strain capacity and the weak cracking resistance of plain concrete. As a result, a more ductile material behaviour can be achieved, leading to growing interests in FRC for a wide range of civil engineering applications, such as ground floors [1–3], precast tunnel segments [4], foundation slabs [5], etc. In the design of FRC elements, the constitutive tensile model is one of the most important models for FRC. Due to this importance, numerous constitutive models have been proposed during the last years [6]. The fib Model Code 2010 (MC10) [7] provides the most recent constitutive tensile models for steel FRC in which the crack bridging effect of the steel fibres is described by specific residual tensile flexural strength values, denoted as f_{R1}–f_{R4}. The magnitude of those parameters depends on the steel fibre type and dosage, concrete mixture proportions and quality [8, 9]. Therefore, multiple empirical approaches [10–14] were proposed to estimate those parameters. The equation proposed by Schultz, as described in Oettel et al. [14], includes the fibre length and considers that the post-cracking performance does not increase linearly with the dosage of fibres. However, Schulz's approach gives the estimation of the residual flexural strength value f_{R4} instead of the residual flexural strength value f_{R3}, as required in the constitutive tensile model in fib MC10 [7]. Therefore, Oettel et al. [14] proposed a modified approach in which the residual flexural tensile strength values f_{R1} and f_{R3} are predicted based on the used steel fibre type and dosage, as well as the concrete mixture. The corresponding formula is given in Eq. (1).

$$f_{Ri} = \frac{1}{0.37}.k.V_f.(1 - k.V_f).\frac{f_{ct,fl}}{0.39}.\zeta_i.\eta_v \tag{1}$$

where f_{Ri} = the residual flexural tensile strength at the specific crack mouth opening displacement (CMOD) values (e.g. $i=1$ for CMOD$_1$ and $i=3$ for CMOD$_3$) (MPa); $f_{ct,fl}$ = flexural tensile strength (MPa); k = factor depending on the fibre type in which $k=5$ for steel chips, $k=9$ for crimped wire strips, and $k=l_f/d_f.\chi$ for steel fibres; l_f = fibre length (mm); d_f = equivalent fibre diameter (mm); χ = factor reflecting the anchoring performance of the fibre with $\chi=0.3$ for hooked-end steel fibres and $\chi = 0.2$ for straight steel fibres; ζ_i = coefficient taking into account the length of the fibres, in which $\zeta_1 = 1.18 + \frac{7.5 l_f}{1000}$ and $\zeta_3 = 0.42 + \frac{7.5 l_f}{1000}$ for the prediction of f_{R1} and f_{R3}, respectively; η_v = coefficient for considering the non-linear influence of the fibre dosage $= 1/(0.7 - 0.2V_f)$.

Nevertheless, in practice, it is often rather hard to establish a correlation between the residual flexural tensile strength of FRC and the required dosage of steel fibres. Therefore, the residual flexural tensile strength values are usually determined by the standardized three-point bending test on notched beam specimens, as given in EN 14651 [15], and the derived magnitude of those parameters is directly used to describe the constitutive tensile model for FRC in MC10 [1]. That constitutive model is divided into two parts: the pre-cracking and post-cracking zone. The pre-cracking zone is entirely determined by the tensile behaviour of plain concrete. The black branch OABC in Fig. 1 represents the constitutive tensile model for plain concrete. The mathematical formulas for those branches are given in Eqs. (2)–(4).

$$\sigma_{ct} = E_{ci}.\varepsilon_{ct} \text{ for } \sigma_{ct} < 0.9 f_{ctm} \tag{2}$$

$$\sigma_{ct} = f_{ctm}\left(1 - 0.1\frac{\varepsilon_P - \varepsilon_{ct}}{\varepsilon_P - 0.9\frac{f_{ctm}}{E_{ci}}}\right) \text{ for } 0.9 f_{ctm} < \sigma_{ct} < f_{ctm} \tag{3}$$

$$\frac{\sigma_{ct} - f_{ctm}}{0.2 f_{ctm} - f_{ctm}} = \frac{\varepsilon_{ct} - \varepsilon_p}{\varepsilon_Q - \varepsilon_p} \text{ for } \varepsilon_P < \varepsilon_{ct} < \varepsilon_Q \tag{4}$$

where σ_{ct} = tensile stress (MPa); f_{ctm} = mean uniaxial tensile strength (MPa); $\varepsilon_Q = \frac{G_F}{f_{ctm}.L_{cs}} + \left(\varepsilon_p - 0.8\frac{f_{ctm}}{E_{cm}}\right)$; G_F = fracture energy of plain concrete (N/m) = $73 f_{\text{cm}}^{0.18}$; f_{cm} = mean cylinder compressive strength (MPa); ε_{ct} = tensile strain (−); ε_p = strain at peak stress = 0.00015 (−); $E_{\text{ci}} = E_{\text{cm}}$ = modulus of elasticity (MPa); s_{rm} = mean distance between cracks (mm); y = distance between the neutral axis and the bottom of the tensile side of the cross-section (mm) corresponding to the serviceability state, as indicated by y_1 in Fig. 1; L_{cs} = structural length (mm), which is equal to min(s_{rm},y) for FRC concrete with conventional rebars.

In addition, MC10 [7] distinguishes two simplified post-cracking constitutive models: the rigid plastic model and the linear (hardening or softening) model. The linear branch of the softening model is characterized by two characteristic points, i.e., $D(\varepsilon_{\text{CMOD1}}, f_{\text{Fts}})$ and $E(\varepsilon_{\text{CMOD3}}, f_{\text{Ft2.5}})$, as given in Fig. 1. The strain at 0.5 mm CMOD ($\varepsilon_{\text{CMOD1}}$) and 2.5 mm CMOD ($\varepsilon_{\text{CMOD3}}$) are described by CMOD$_1$/$L_{\text{cs}}$ and CMOD$_3$ /L_{cs}, while the corresponding equations for the residual flexural tensile strength at SLS and ULS are given by Eqs. (5)–(6) [7]. For thin-walled elements, a shift of the f_{Fts} value to CMOD = 0 mm prevents some spurious situations where a class reduction could involve a better performance in bending. Therefore, the stress profile at ULS in MC10 considers that f_{Fts} is associated with CMOD = 0 mm.

$$f_{\text{Fts}} = 0.45 f_{R1} \quad (5)$$

$$f_{\text{Ftu}} = f_{\text{Fts}} - \frac{w_u}{\text{CMOD}_3}\left(f_{\text{Fts}} - 0.5f_{R3} + 0.2f_{R1}\right) \geq 0 \quad (6)$$

where f_{Fts}= tensile strength at SLS (MPa); f_{Ftu}= tensile strength at ULS (MPa); f_{R1} and f_{R3} are the residual flexural tensile strengths (MPa) at 0.5 mm CMOD (= CMOD$_1$) and 2.5 mm CMOD (= CMOD$_3$), according to EN 14651 [15]; w_u = maximal accepted crack opening (mm), ranging between CMOD$_1$ and CMOD$_3$.

To better explain the concepts of the constitutive tensile model for FRC in MC10, di Prisco et al. published a new paper in 2013 [16], in which f_{Fts} was modified to 0.37 f_{R1} at 0.5 mm CMOD. The value 0.37 will also be used to calculate the effective tensile strength at SLS (CMOD$_1$) according to Annex L of the next version of Eurocode 2 (EC2) [17], as given in Eq. (7). The effective tensile strength at CMOD$_3$ will then be computed with Eq. (8).

$$f_{\text{Ft1,ef}} = \kappa_o \kappa_G 0.37 f_{R,1k} \quad (7)$$

$$f_{\text{Ft3,ef}} = \kappa_o \kappa_G (0.57 f_{R,3k} - 0.26 f_{R,1k}) \quad (8)$$

where $f_{R,1k}$ = characteristic residual flexural tensile strength at 0.5 mm CMOD (MPa); $f_{R,3k}$ = characteristic residual flexural tensile strength at 2.5 mm CMOD (MPa); κ_o is a function of the fibre orientation and is equal to 1 for randomly distributed fibres; κ_G is correlated to the size of the volume involved in the cracked procedure and can be approximated to 1 for prismatic specimens (EN 14651).

It should be noted that the post-cracking strength of FRC is generally classified based on their characteristic residual flexural strength values at CMOD$_1$ and CMOD$_3$, as given in MC10 [7]. More precisely, the FRC performance class is described by f_{R1k} (representing the strength interval) and a letter *a, b, c, d,* or *e* (representing the f_{R3k}/f_{R1k} ratio). The strength interval is defined by two subsequent numbers in the series: 1.0, 1.5, 2.0, 2.5, 3.0, 4.0, 5.0, 6.0, 7.0, 8.0, … (MPa), while the letters *a, b, c, d, e* correspond to the following residual strength ratios: *a* if $0.5 < f_{R3k}/f_{R1k} < 0.7$; *b* if $0.7 \leq f_{R3k}/f_{R1k} < 0.9$; *c* if $0.9 \leq f_{R3k}/f_{R1k} < 1.1$; *d* if $1.1 \leq f_{R3k}/f_{R1k} < 1.3$; and *e* if $1.3 \leq f_{R3k}/f_{R1k}$. Despite this classification, the models shown in Eqs. (5)–(8) in MC10 [7] and EC2 (next generation) [17] do not make a distinction for a specific f_{R3k}/f_{R1k} ratio.

2 New constitutive tensile models

The investigated glass FRC mixtures (GFRC) and polypropylene FRC (PFRC) mixtures in the research work of Vandevyvere at KU Leuven [18] revealed that the constitutive tensile models for FRC in MC10 [7, 19] can be further optimized to better describe the post-cracking behaviour of this material. The used FRC mixtures in [18] have a concrete compressive strength (f_{cm}) between 40 and 56 MPa and the Young's modulus (E_{cm}) ranges from 27 to 43 GPa. In addition, the measured f_{R1}- and f_{R3}-values are located in the range 1.4–4.2 and 0.9–3.9 MPa, respectively, mainly depending on the volume content of the fibres. It was observed that a similar bilinear stress–strain relation can be used in the pre-cracking stage, as given in MC10, see Eqs. (2)–(3). However, the sectional analysis results indicated that more accurate results can be achieved when the peak strain (ε_P) in the model is assumed to be 0.010% instead of 0.015% [18, 19], while for the post-peak branch of plain concrete, the same formula, i.e., Eq. (3) can be used. Next to this, it was found that a distinction can be made between the post-cracking branch in the constitutive tensile model for different FRC performance classes. The general equations to describe this linear post-cracking branch are given by Eq. (9) and (10), in which different k'_a and k'_c -values must be applied for different FRC classes [20]. As a starting point, the k'_a and k'_c -values are derived by a simplified stress profile at CMOD$_1$ and CMOD$_3$ [20]. Both stress profiles neglect the concrete tensile stress and assume a linear stress–strain relation for concrete in compression

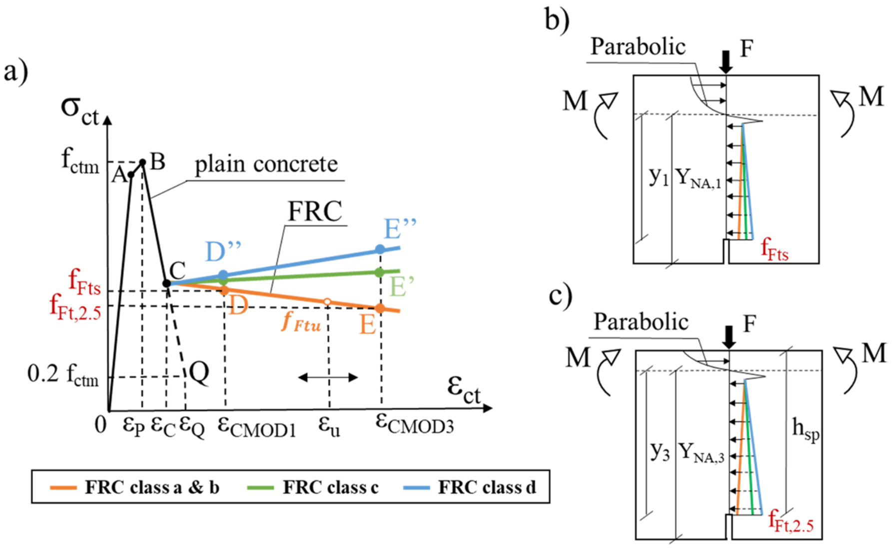

Fig. 1 Tensile stress–strain model for different FRC classes (**a**), with the indication of the used stress and strain profile at $CMOD_1$ (**b**) and $CMOD_3$ (**c**) in the new constitutive tensile models

[18], which are similar to MC10 [7] and di Prisco et al. [16].

$$f_{\mathrm{Fts}} = k'_a f_{R1} \tag{9}$$

$$f_{\mathrm{Ftu}} = f_{\mathrm{Fts}} - \frac{w_u}{\mathrm{CMOD}_3}\left(f_{\mathrm{Fts}} - \frac{125^2}{2.y^2} f_{R3} + \frac{k'_c}{2} f_{R1}\right) \geq 0 \tag{10}$$

where k'_a and k'_c are specific design parameters; y is the tensile zone depth at $CMOD_3$ (mm), as indicated by y_3 in Fig. 1.

However, it was found that the k'_a- and k'_c-values can be further optimized to improve the predictive accuracy of the models [20]. The optimization was done by using the inverse analysis procedure [18], in which the k'_a- and k'_c-values were numerically optimized until a relative error ΔE smaller than 1% was obtained at $CMOD_1$ and $CMOD_3$. In this optimization [19], the concrete tensile strength (f_{ctm}) and the parabolic compressive stress–strain model for concrete under compression, as recommended in MC10 [7], was included in the stress profile (at $CMOD_1$ and $CMOD_3$, see Fig. 1) [19]. It should be pointed out that existing standards typically neglect the contribution of the uncracked tensile zone, aligning with the assumption of conventional reinforced concrete structures. This is because the contribution of the uncracked tensile zone is often much less than that of steel rebars. However, in case of FRC without steel rebars, the incorporation of the concrete tensile strength is reasonable because it is much closer to the tensile contribution of the fibres, and consequently, the concrete tensile strength was included in the optimized stress profiles, as published in [19]. In addition, this contribution can also be considered in case the structural member is subjected to the first loading condition or the member is not originally cracked for other reasons. Eqs. (11)–(12) give the derived optimized post-cracking branch for FRC class *a* and *b* [19], while the corresponding equations for FRC class *c* and *d* are described in Eqs. (13)–(14) and Eqs. (15)–(16), respectively [18]. Figure 1 presents a graphical illustration of the three new models.

- FRC class *a* & *b*:

$$f_{\mathrm{Fts}} = 0.34 f_{R1} \tag{11}$$

$$f_{\mathrm{Ftu}} = f_{\mathrm{Fts}} - \frac{w_u}{\mathrm{CMOD}_3}\left(f_{\mathrm{Fts}} - 0.57 f_{R3} + 0.35 f_{R1}\right) \geq 0 \tag{12}$$

- FRC class *c*:

$$f_{\mathrm{Fts}} = 0.37 f_{R1} \tag{13}$$

$$f_{\mathrm{Ftu}} = f_{\mathrm{Fts}} - \frac{w_u}{\mathrm{CMOD}_3}\left(f_{\mathrm{Fts}} - 0.56 f_{R3} + 0.15 f_{R1}\right) \geq 0 \tag{14}$$

- FRC class *d*:

$$f_{\mathrm{Fts}} = 0.41 f_{R1} \quad (15)$$

$$f_{\mathrm{Ftu}} = f_{\mathrm{Fts}} - \frac{w_u}{\mathrm{CMOD}_3}\left(f_{\mathrm{Fts}} - 0.58 f_{R3} + 0.09 f_{R1}\right) \geq 0 \quad (16)$$

As can be seen from the equations above, a higher performance class has a higher k_a'-value, while the k_c'-value significantly decreases for FRC of a higher performance class. The proposed tensile model for FRC class *a* and *b* was developed based on the test data from a total of 62 notched GFRC specimens, while the models for FRC class *c* and *d* were established using 12 PFRC notched beam specimens for each FRC class. Also two different types of PP fibres were used for those two FRC classes. The geometrical and mechanical properties of the used glass fibres (M1) and the two PP fibres (M2 and M3) are given in Table 1. The longer length of the M3 fibre, compared to M2, results in an improved crack-bridging effect which slightly increases the $\frac{125^2}{2.y^2}$ ratio. Therefore, the $\frac{125^2}{2.y^2}$ ratio increases from 0.56 for FRC class *c*, see Eq. (14) to 0.58 for FRC class *d* as shown in Eq. (16). Those values slightly differ from the proposed value (0.57) of EC2, while the $\frac{125^2}{2.y^2}$ ratio for FRC performance class *a* and *b* is similar as that in EC2, as shown in Eq. (8).

3 Objective and methodology

Nowadays, a wide range of macro fibres has been developed to reinforce the plain concrete matrix. Therefore, the objective of this paper is to examine if Oettel's estimation model for the post-cracking behaviour (Eq. (1)) as well as the new constitutive tensile models (Sect. 2) can be used for FRC mixtures with other types of macro fibres (with different geometrical and mechanical properties) than the used fibres in the construction of the models. To this end, a database was constructed in which the test data from two sources was gained: (a) from the publication of Vrijdaghs et al. [21]; (b) from the international company Bekaert. The whole database consists of 23 FRC mixtures with 6 different types of macro fibres (steel fibres and PP fibres). In total, 236 notched beam specimens are included. Detailed information of the fibres and concrete properties, included in the database, is given in Sect. 4. However, not all the collected test data was included in the verifications. More precisely, a distinction is made as follows:

(1) Verification of the model of Oettel et al. [14]

The estimation formula of Oettel et al. (Eq. (1)) was established based on test data on steel fibre reinforced concrete, in which the fibre length, fibre diameter, fibre anchorage, fibre content, and the concrete flexural tensile strength are directly incorporated in the model. However, previous research [22, 23] showed that a well-designed fibre anchorage system significantly affects the measured residual flexural tensile strength values of FRC. The 4D Dramix fibres, developed by Bekaert, have been found to be able to significantly enhance the post-cracking behaviour owing to its double-bended anchorage system. Because of this, the model of Oettel et al. [14] is only verified for this specific steel fibre type in this paper. Consequently, a total of 204 notched beam specimens are included in this verification.

(2) Verification of the new constitutive tensile models [18]

In the new constitutive tensile models (see Sect. 2), the experimental residual tensile strength values f_{R1} and f_{R3} are directly incorporated. Therefore, the impact of the fibre type (and its mechanical behaviour) is directly reflected in the model. From this perspective, all the FRC specimens collected in the database, i.e., 236 notched beams, corresponding to a certain FRC performance class, are included in the verification of the new constitutive models.

To check the validity of the different models, the experimental values of the residual flexural tensile strength (e.g. f_{R1} and f_{R3}) are compared with the predicted values of the residual flexural tensile strength. Therefore, the statistical analysis on the ratio of the predicted values ($f_{R1,\mathrm{pred}}$ or $f_{R3,\mathrm{pred}}$) to the experimentally observed values (denoted as $f_{R1,\mathrm{exp}}$ and $f_{R3,\mathrm{exp}}$) is carried out. The calculated statistical parameters include the expected value $E(X)$ (= mean value of $f_{R1,\mathrm{pred}}/f_{R1,\mathrm{exp}}$ or that of $f_{R3,\mathrm{pred}}/f_{R3,\mathrm{exp}}$), the standard deviation (s), the coefficient of variation (CoV), and $Q_{0.05}$ and $Q_{0.95}$ denoting the 5 and 95% quantiles, respectively.

4 Database

4.1 Fibre and concrete properties

The collected test data for the model verifications includes three macro steel fibres (S1, S2, and S3), and three types of macro PP fibres (PP1, PP2, and PP3). The geometrical and mechanical properties of the fibres are given in Table 1. Note that the used steel fibres S2 and S3 are 4D Dramix fibres, while the fibre anchorage system of the S1 fibres is not mentioned in [21].

Table 2 gives an overview of the used fibre content and the number of notched beam specimens that are used in the model verifications in this paper. The specimens from Bekaert were tested at a curing age of 7 or 28 days, while all specimens of Vrijdaghs et al. [21] were tested after 28 days. Next to this, the corresponding FRC class for every mixture is also included in the same Table, in which the characteristic residual flexural tensile strength values (f_{Rk}) are calculated by assuming a lognormal distribution in accordance with Eqs. (17)–(19). It must be noted that in some mixtures the f_{R1k} is too small (< 1 MPa) and could not be classified, as indicated by the abbreviation "NC" in Table 2. Nevertheless, those mixtures are also included in the model verifications since the f_{R3k}/f_{R1k} ratio is defined.

$$f_{Rk} = \exp(f_{\ln,m} - k_n \cdot \sigma_{\ln}) \tag{17}$$

$$f_{\ln,m} = \frac{1}{n} \cdot \sum_{i}^{n} \ln f_i \tag{18}$$

$$\sigma_{\ln} = \sqrt{\frac{1}{n-1} \cdot \sum_{i}^{n} \left(\ln f_i - f_{\ln,m}\right)^2} \tag{19}$$

where $f_{\ln,m}$ = the mean value of the natural logarithm of the relevant residual strength values, k_n = the 5% quantile factor, which is dependent on the number of specimens (n) and the variation coefficient which is not known before the test. The k_n-factor can be found in Table D1 of EN 1990 [24].

For all the FRC mixtures, the compressive strength was determined according to EN 12390-3 [25]. The measured cube compressive strength (dimension: 150 × 150 × 150 mm^3) of the FRC mixtures tested at Bekaert is given in Fig. 2. In this figure, the different concrete mixtures are denoted by a specific letter, and the corresponding fibre content for each mixture is given in Table 2. It should be noted that only for mixture O, the concrete compressive strength was not measured. The compressive strength of the FRC mixtures tested by Vrijdaghs et al. [21] ranges from 42 to 60 MPa. However, the compressive strength of each individual FRC mixture is not given in [21]. Due to this reason, the uniaxial tensile strength, compressive strength, and E-modulus of all the FRC mixtures are also calculated by using the proposed equations in MC10 [7], as given in Eqs. (20), (21), and (22). To

Table 1 Geometrical and mechanical properties of the used fibres in concrete properties

	Purpose	Fibre type	Shape	Length (mm)	Equivalent diameter (mm)	Tensile strength (MPa)	E-modulus (MPa)
M1	CCM	Glass fibres	Straight, twisted helix	43	0.70	> 1000	42,000
M2	CCM	Polypropylene fibres	Straight, embossed	45	0.90	451	3350
M3	CCM	Polypropylene fibres	Straight, embossed	55	0.70	417	5740
S1	VCM	Steel fibres	Hooked end	50	0.80	1200	210,000
S2	VCM/VOM	Steel fibres	Hooked end	50	0.90	1600	200,000
S3	VCM/VOM	Steel fibres	Hooked end	50	0.75	1800	200,000
PP1	VCM	Polypropylene fibres	Embossed	55	0.90	465	3350
PP2	VCM	Polypropylene fibres	Twisted bundle monofilament	54	0.80	620	9500
PP3	VCM	Polypropylene fibres	Crimped	40	0.77	400	5000

CCM = Construction of the new Constitutive Models [18]; *VCM* = Verification of the new Constitutive Models; *VOM* = Verification of the Model developed by Oettel et al. [14]

Table 2 Overview of the fibre content and the corresponding FRC class of the included FRC mixtures in the model verifications, in which the mixture abbreviation (if applicable), the number of notched beam specimens, and the curing period are included in brackets

	Vrijdaghs [21]	Bekaert	FRC class
S1	0.20 V% (5 beams–28 days)	–	1.5 a
S2	–	15 kg/m³ (F—12 beams–7 days)	NC (< 1 c)
	–	20 kg/m³ (G—12 beams–7 days)	1 c
	–	20 kg/m³ (N—11 beams–28 days)	1 c
	–	25 kg/m³ (O—12 beams–28 days)	1 c
	–	30 kg/m³ (H—12 beams–7 days)	1 d
	–	30 kg/m³ (P—12 beams–28 days)	1.5 c
	–	35 kg/m³ (I—12 beams–7 days)	2 d
	–	35 kg/m³ (Q—12 beams–28 days)	2 c
S3	–	15 kg/m³ (A—12 beams–7 days)	NC (< 1 d)
	–	15 kg/m³ (J—12 beams–28 days)	1 c
	–	20 kg/m³ (B—12 beams–7 days)	1 d
	–	20 kg/m³ (K—12 beams–28 days)	1.5 d
	–	25 kg/m³ (C—12 beams–7 days)	1 d
	–	25 kg/m³ (L—12 beams–28 days)	2 d
	–	30 kg/m³ (D—12 beams–7 days)	1.5 d
	–	30 kg/m³ (M—12 beams–28 days)	2 d
	–	35 kg/m³ (E—12 beams–7 days)	2 d
PP1	0.45 V% (6 beams–28 days)	–	NC (< 1 a)
PP2	0.45 V% (6 beams–28 days) 1.00 V% (6 beams–28 days)	–	1 a 1.5 b
PP3	0.45 V% (5 beams–28 days) 1.00 V% (5 beams–28 days)	–	NC(< 1 b) 1.5 c

NC = not classified

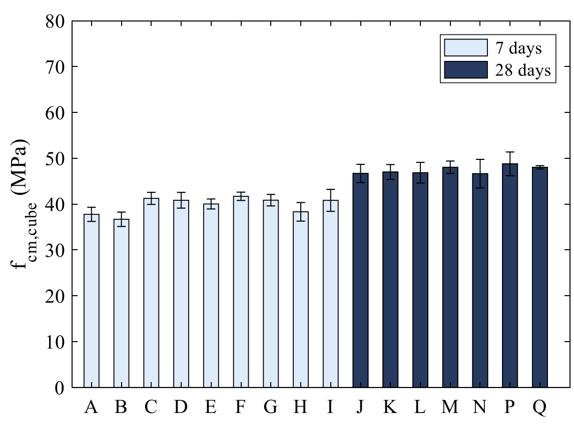

Fig. 2 Measured compressive strength of the FRC mixtures tested at Bekaert

obtain similarity, those computed values are used in the verifications of the models.

$$f_{ctm} = \frac{0.06h_{sp}^{0.7}}{1 + 0.06h_{sp}^{0.7}} f_{ctm,fl} \tag{20}$$

$$f_{ck,cyl.} = f_{cm} - 8 = \left(\frac{f_{ctm}}{0.3}\right)^{3/2} \tag{21}$$

$$E_{cm} = E_{c0}.\alpha_E.\left(\frac{f_{cm}}{10}\right)^{1/3} \tag{22}$$

where $f_{ctm,fl}$ = mean tensile strength due to the presence of the notch (MPa) ≈ limit of proportionality (MPa), according to EN 14651 [15]; f_{ctm} = mean uniaxial tensile strength (MPa); f_{cm} = mean cylinder compressive strength (MPa) and $f_{ck,cyl.}$ = characteristic cylinder compressive strength (MPa); α_E = factor depending on the aggregate type (≈ 1.0); E_{co} = 21.5 × 10^3 MPa; h_{sp} = notched beam height (= 125 mm).

4.2 Monotonic bending test

The post-cracking behaviour of all the collected FRC mixtures was investigated according to EN 14651 [15], in which the notched beam specimens were subjected to a displacement-controlled three-point bending. All FRC mixtures were cast in rectangular moulds with a cross-section of 150 × 150 mm^2, and a length of 600 mm. Those beams were stored in a climate chamber at a temperature of 20 ± 2 °C and relative humidity > 95% until a few days before testing. After the curing period, a notch of 25 mm was sawn at midspan of the beams. The three-point bending tests were performed in two laboratories, namely in the laboratory of the Belgian Building Research Institute (BBRI) and in the laboratory at Bekaert, as indicated in Table 2. At BBRI, a constant loading rate of 0.05 mm/min was firstly used up to a midspan deflection of 0.125 mm, then it was changed to 0.17 mm/min until the end of the test. Those midspan deflections were measured by two linear variable displacement transducers (LVDT) attached at each side of the specimens. In the Bekaert laboratory, a constant loading rate of 0.0425 mm/min was used for a midspan deflection ranging from 0 to 0.125 mm, while a constant rate of 0.17 mm/min was used to the end of the test. In addition, the midspan deflection was measured by the use of one LVDT at the moulded side of the specimens. It should be noted that the CMOD-values at BBRI were measured exactly at the bottom side of the specimens, while that of the specimens tested at Bekaert were calculated based on the measured midspan deflections of the beams, using the equation given in EN 14651 [15]. This calculation was done because the CMOD-values were not directly measured during the testing. At BBRI, a total of 7 LVDTs were also glued to one side of the beam at 7, 23, 55, 69, 83, 99, and 115 mm from the bottom of the specimens [21]. Those LVDTs were used to locate the neutral axis of the beam cross-section at midspan at a specific CMOD-value. In general, it can be concluded that the 236 monotonic bending test results are located between the boundaries $f_{R3}/f_{R1} = 0.5$ and $f_{R3}/f_{R1} = 1.5$, respectively (as shown in Fig. 3). Moreover, by considering the characteristic residual flexural tensile strength values, all FRC mixtures can be classified into performance class *a, b, c,* or *d*.

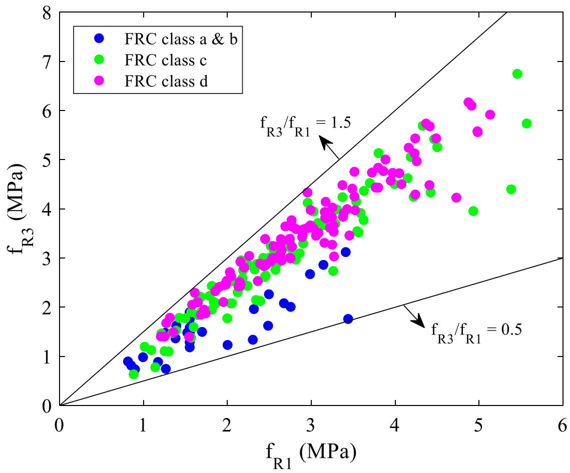

Fig. 3 Boundaries of the f_{R1} and f_{R3} values of the collected FRC mixtures

5 Comparison between model predictions and test data

5.1 Empirical formula of the residual flexural tensile strength

The model proposed by Oettel et al. for predicting the residual flexural tensile strength of FRC, as shown in Eq. (1), was developed based on three-point bending tests in accordance with EN 14651 [15]. The steel fibres used in the FRC mixtures for establishing the model have hooked-ends, a length between 25 and 80 mm, a diameter between 0.2 and 1.2 mm, an aspect ratio between 37.5 and 120, and a tensile strength ranging from 1100 to 3100 MPa. The fibre content varied from 0.1 to 2.0 V% and the concrete cylinder compressive strength was between 24 and 108 MPa, while the flexural tensile strength of the concrete was in the range of 2.5–8.5 MPa.

Figure 4a–b compare the experimentally observed f_{R1} and f_{R3}-values with the predictions of Oettel's model [14] for the tested FRC specimens with the collected 4D Dramix fibres in the database. As can be seen from the figures, all specimens can be classified into FRC class *c* or *d*, and a weak correlation is generally found between the measured values and the model predictions for both residual flexural tensile strength, i.e., f_{R1} and f_{R3}, irrespective of FRC performance class. The expected value $E(x)$, which represents the mean value of the predicted to experimental

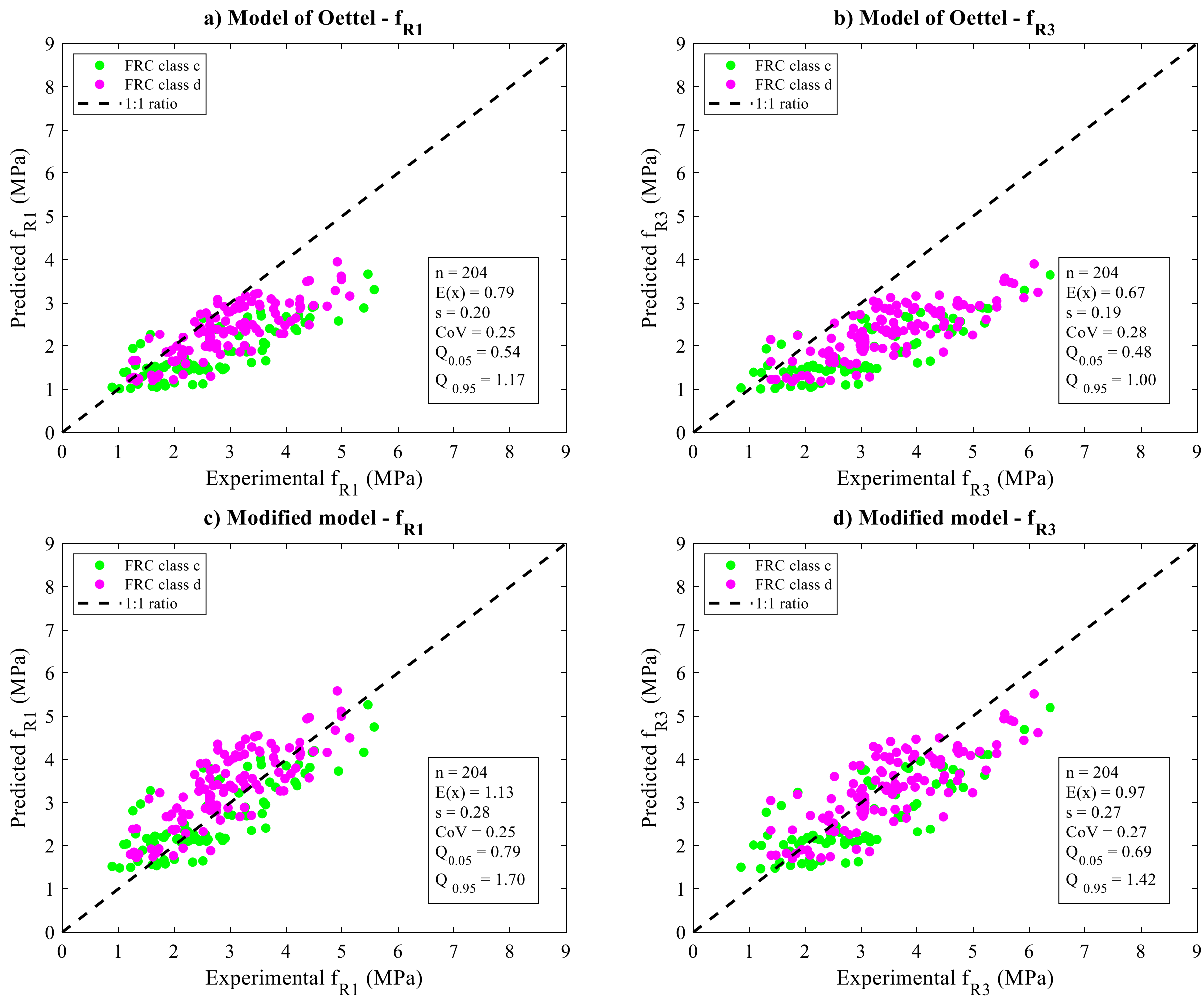

Fig. 4 Comparison between the experimental f_{R1} or f_{R3}-values, and predicted f_{R1} or f_{R3}-values according to Oettel's model (**a**–**b**) and the modified model (**c**–**d**), by including the fibre reinforced concrete specimens with the 4D Dramix fibres

residual flexural tensile strength ratio at $CMOD_1$ and $CMOD_3$ for both FRC classes, is found to be 0.79 and 0.67, respectively. This indicates that the model of Oettel et al. [14] underestimates the residual flexural tensile strength values of the FRC mixtures, implying that the model predictions tend to be conservative.

Due to the limited test data of FRC specimens with non-Dramix fibres, it is hard to conclude whether the model of Oettel et al. [14] is also conservative for FRC mixtures with other types of steel fibres. The main reason for the underestimation of the residual flexural tensile strengths of the FRC mixtures with 4D Dramix fibres, is believed to be due to the less adequate consideration of the fibre anchorage in the model. As shown in Eq. (1), the χ-factor does not differ for FRC mixtures with a single and a double bending at the end of the fibres. To improve the predictive accuracy, the value of the χ-parameter in the original model of Oettel et al. [14] is optimized for the FRC mixtures with 4D Dramix fibres, taking into account the specific double-bended anchorage system of this type of fibres. This was done by using the least-square method. The optimization yields a new χ-value for FRC with 4D Dramix fibres, which is $\chi = 0.44$. A comparison between the experimentally observed f_{R1}- and f_{R3}-values and the predictions of the model of Oettel et al. [14] with $\chi = 0.44$ is shown in Fig. 4c–d. It can be seen from the figures that the modifications of the original model yield a better prediction of the f_{R1} and f_{R3}-values of the FRC mixtures.

The mean value of the predicted to the measured residual flexural tensile strength ratio at $CMOD_1$ and $CMOD_3$ for both FRC classes (i.e., *c* and *d*) is 1.13 and 0.97, respectively. However, a high scattering is still observed between the experimental and predicted f_{R1} and f_{R3}-values, which is believed to be mainly attributed to the randomness of the fibre distribution in the concrete mixtures [26].

5.2 New constitutive tensile models

5.2.1 The sectional analysis

To verify the new and existing constitutive tensile models (see Sect. 2), a layer-by-layer sectional analysis, formerly applied by Kooiman [27], was performed on the test data of Vrijdaghs et al. [21] and Bekaert (see Sect. 4). The analysis is based on a plane section approach, and consequently, any non-linearity in the strain distribution along the height of the cross-section is neglected. The procedure of the used sectional analysis in this paper can be summarized in the following five steps:

- The cross-section of the notched beam is divided into 125 layers with a height of 1 mm for each layer. Those layers are connected above the notch by virtual springs. In this way, the total beam response is determined by all springs together [28].
- To transform the crack opening to an equivalent tensile strain and equivalent compressive strain, the relationship between strain and crack opening is needed. In this paper, the transformation is made by the use of a fictitious length method and is determined by the ratio between CMOD and the structural length (L_{cs}), according to MC10 [7]. In MC10, the parameter L_{cs} is defined as the minimum of the average crack distance (s_{rm}) and the tensile zone length at SLS (*y*). It is important to note that the parameter L_{cs} is not a static parameter but may evolve in the different load steps. Despite this variability, the plane section approach admits only two kinematic parameters: the centre of gravity strain and the curvature which are the same for all the fibres of the section that remains plane in the generic load step. Consequently, L_{cs} is always considered equal to the notched beam height (h_{sp} = 125 mm) in a specific load step. This assumption is in line with MC10 for FRC sections under bending without containing traditional reinforcement [7]. Similar method was also used in [29, 30].
- Stresses in the tension and compression zones of the cross-section are determined by the pre-defined constitutive laws. In this approach, the experimental tensile stress-CMOD curves can be verified with the new and existing constitutive tensile models, as described in Sect. 1. For the new constitutive tensile models, the peak strain (ε_P) in the constitutive tensile model for FRC, as shown in Eqs. (2)–(4) is assumed to be 0.010%, and the newly developed post-peak branches in Eqs. (11)–(16) are used to describe the post-cracking behaviour of FRC (according to the performance class). In the compression zone of the beam cross-section, the uniaxial compressive stress–strain model of MC10 [7] is applied to determine the compressive stress according to the concrete compressive strain, as shown in Eq. (23). A similar stress profile at $CMOD_1$ and $CMOD_3$ as in Fig. 1 is also used to verify the model of EC2 and MC10, and consequently the assumed simplification in the stress profile of the standards are not considered to be in line with the newly developed model.

$$\frac{\sigma_c}{f_{cm}} = -\left(\frac{k.\eta - \eta^2}{1 + (k-2).\eta}\right) \quad \text{for} \left|\varepsilon_c\right| < \left|\varepsilon_{c,\lim}\right| \tag{23}$$

where $\eta = \varepsilon_c / \varepsilon_{c1}$ (−); $k = E_{ci}/E_{c1}$ (−); ε_c = compressive strain (−); ε_{c1} = compressive strain at f_{cm} (−); f_{cm} = mean cylinder compressive strength (MPa); E_{c1} = secant modulus from the origin to f_{cm}; $E_{ci} = E_{cm}$ = the modulus of elasticity (GPa).

- The assumed neutral axis location is changed iteratively to obtain the horizontal force equilibrium. The resulted horizontal force(ΔH) is calculated according to Eq. (24), which must be equal to zero in order to obtain equilibrium.

$$\Delta H = b.\left[\int_{25\text{mm}}^{Y_{\text{NA}}} \sigma_{ct}\left(\varepsilon_{ct}\right)dy + \int_{Y_{\text{NA}}}^{h} \sigma_c\left(\varepsilon_c\right)dy\right] \approx \sum_{i=1}^{n} \sigma_i.\Delta h.b = 0 \tag{24}$$

where b = beam width (150 mm); Y_{NA} = location of the neutral axis; h = beam height (150 mm); $\sigma_c\left(\varepsilon_c\right)$ = compressive stress determined by the compressive constitutive model of MC10 [7] and $\sigma_{ct}(\varepsilon_{ct})$ = tensile stress determined by one of the new or existing constitutive tensile models; Δh = height of one layer = 1 mm and σ_i = the mean tensile or compressive stress in the *i*th layer.

- Once the horizontal force equilibrium ($\Delta H = 0$) is satisfied, the corresponding compressive and tensile stresses can be used to calculate the bending moment M_{cal}, according to Eq. (25). Consequently, the residual flexural tensile strength at a specific CMOD-value can be identified.

$$M_{\mathrm{cal}} = b.\left[\int_0^{Y_{\mathrm{NA}}} \sigma_{ct}(\varepsilon_{ct}).(Y_{NA} - y)dy + \int_{Y_{\mathrm{NA}}}^{h} \sigma_c(\varepsilon_c).(y - Y_{\mathrm{NA}})dy\right] \approx \sum_{i=1}^{n} \sigma_i.y_i.\Delta h.b \tag{25}$$

where y_i = distance from the centroid of layer *i* to the neutral axis.

5.2.2 Tensile stress–CMOD curves

A comparison of the measured and calculated tensile stress–CMOD curves, using the new constitutive tensile models for the different FRC mixtures, is shown in Fig. 5. The solid lines represent the average of the experimental stress-CMOD curves, whereas the dashed lines are the predicted curves by use of the new constitutive tensile models for a specific FRC performance class through the sectional analysis. Overall, a good agreement is found between all experimental and predicted curves.

To better evaluate the predictive accuracy of the newly developed constitutive tensile models for FRC, the absolute errors (ΔE) between the predicted and experimental $f_{ct,fl}$, f_{R1} and f_{R3} values are calculated according to Eq. (26), and the calculated results are shown in Fig. 6.

$$\Delta E = \left| f_{\mathrm{exp}} - f_{\mathrm{pred}} \right| \tag{26}$$

where f_{exp} = experimental (residual) flexural tensile strength (MPa), obtained from the three-point bending test (EN 14651 [15]); f_{pred} = predicted (residual) flexural tensile strength (MPa), by the use of a specific constitutive tensile model (according to the FRC performance class).

As illustrated in Fig. 6a, the use of a peak tensile strain (ε_P) of 0.010% in the constitutive tensile model yields a more accurate prediction of the flexural tensile strength of the specimens, in comparison to the assumption of that parameter as 0.015%, as recommended in MC10 [7]. A similar finding was previously reported in [18]. However, it is noticed that the predicted flexural tensile strength of the FRC mixtures with ε_P = 0.010% still exceed the measured values, which is mainly related to the assumption of a linear deformation profile of the cross-section of the specimens in the pre-cracking stage of the FRC mixtures [18]. The use of a bilinear deformation profile has been found to be able to improve the predictive accuracy of the calculations [18]. In addition, Fig. 6b indicates that the median of the calculated absolute error for the f_{R1}-values only ranges between 0.06 and 0.14 MPa, depending on the FRC performance class. However, the absolute error of the f_{R3}-values increases for a higher FRC class, but its value is still relatively small (with the median smaller or equal to 0.49 MPa).

Due to the high accuracy of the new constitutive tensile models, the 236 beam specimens also show a good 1:1 ratio between the experimental and predicted f_{R1} or f_{R3}-values. This is visualized in Fig. 7. Logically, the highest deviation between the predicted and experimental f_{R3}-values is also observed for FRC performance class *d*.

The statistical parameters for evaluating the predictive accuracy of the new constitutive tensile models, as shown in Fig. 7, are also summarized in Table 3. Since the statistical analysis is carried out to verify the accuracy of the predicted models, the expected value $E(x)$ (i.e. mean value of the ratio $f_{R1,\mathrm{pred}}/f_{R1,\mathrm{exp}}$ or $f_{R3,\mathrm{pred}}/f_{R3,\mathrm{exp}}$) should be close to 1.00, when the models are realistic. In addition, a small standard deviation (s) or a low coefficient of variation (CoV), and a narrow band in $Q_{0.05}$ and $Q_{0.95}$ are needed to ensure the reliability.

As can be seen from Table 3, the new model for FRC class *a* and *b* indicates an $f_{R1,\mathrm{pred}}/f_{R1,\mathrm{exp}}$ and $f_{R3,\mathrm{pred}}/f_{R3,\mathrm{exp}}$ ratio of 1.04 and 0.86, respectively. A higher accuracy is observed for FRC class *c*, as revealed by an expected value closer to 1 at CMOD_1 and CMOD_3 than for FRC class *a* and *b*. In spite of an increased deviation between the predicted and

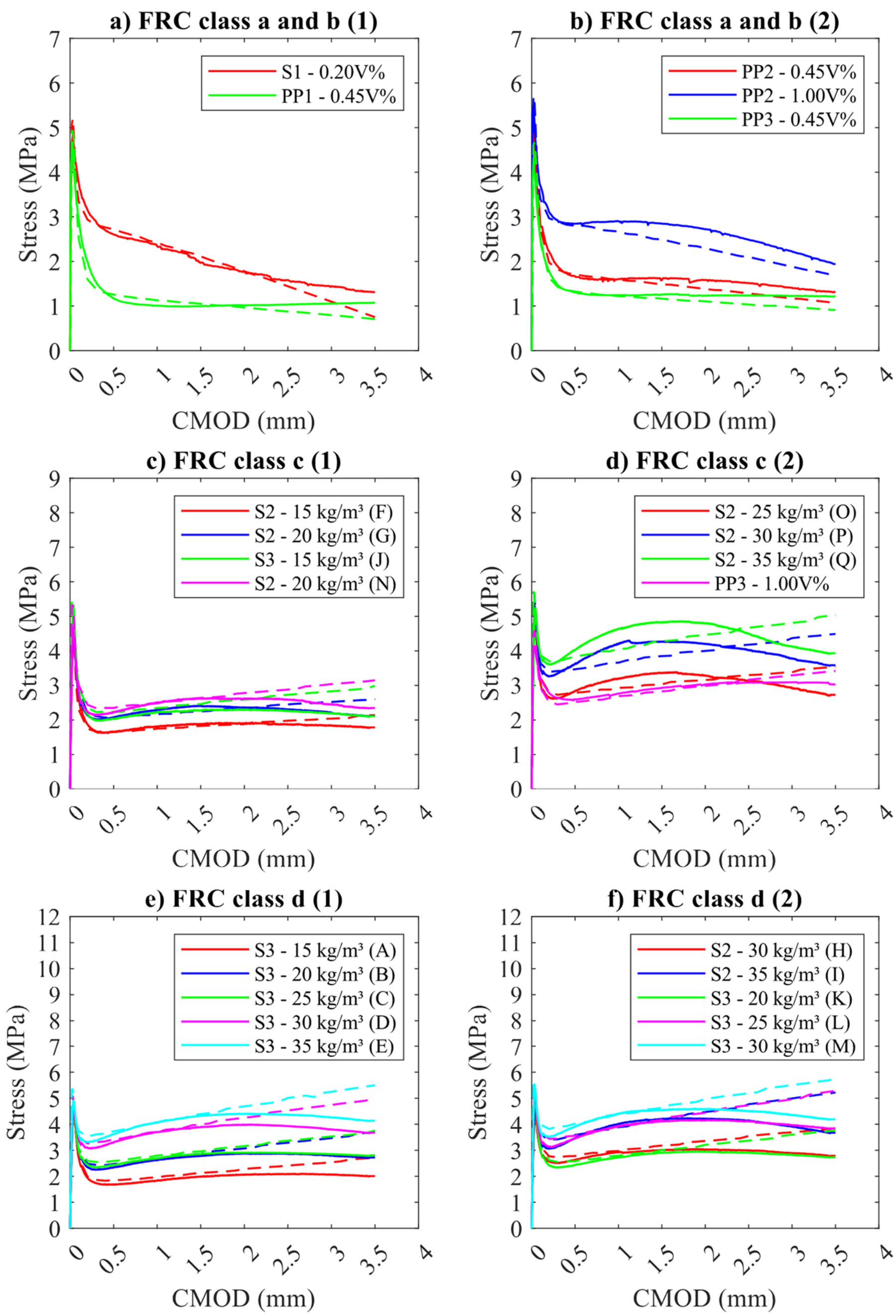

Fig. 5 Comparison of the mean experimental (solid line) and the predicted stress-CMOD curve with the new constitutive tensile models (dashed line) for the FRC mixtures

measured residual flexural tensile strength values at $CMOD_3$ for FRC class *d*, a high accuracy at $CMOD_1$ is also obtained for this specific FRC class. Table 3 also includes the statistical parameters for the predicted and experimental residual flexural tensile strength values, when the constitutive tensile model in MC10 [7] and EC2 (next generation) [17] are used. As can be seen, the new constitutive tensile model for FRC class *a* and *b* as well as FRC class *c* has a higher accuracy than the proposed model of MC10 [7] and EC2 [17] at $CMOD_1$.

Furthermore, the $Q_{0.05}$–$Q_{0.95}$ band for the ratio of the predicted residual flexural tensile strength to the experimental strength for FRC class *a* & *b*, especially at $CMOD_3$-values, is significantly smaller than that with the models in MC10 [7]

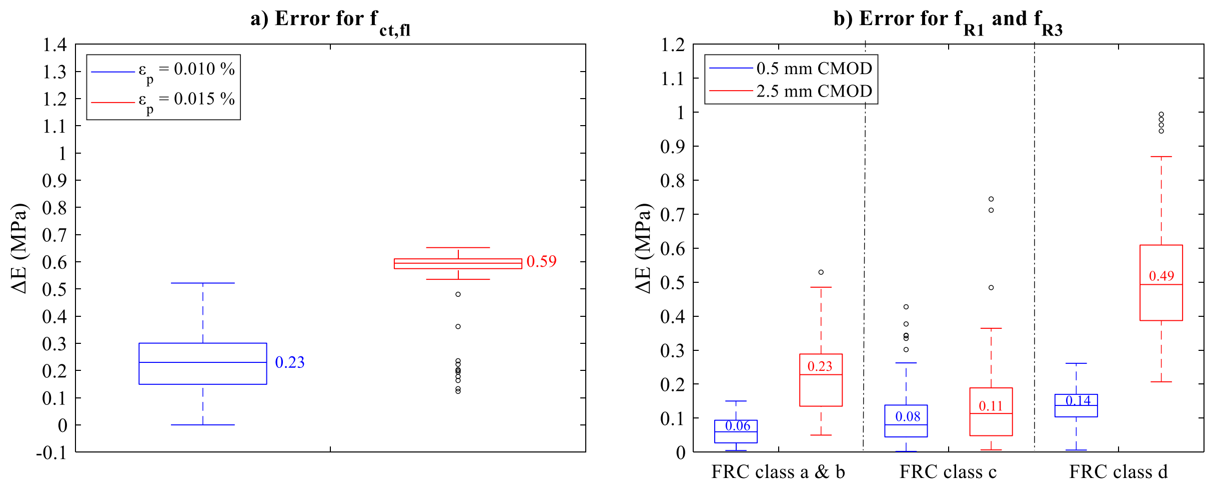

Fig. 6 Deviation of the experimental and the predicted $f_{ct,fl}$-value, with $\varepsilon_p = 0.010\%$ and $\varepsilon_p = 0.015\%$ (**a**); Deviation (in MPa) of the experimental and predicted f_{R1} or f_{R3}-values with the new constitutive tensile models for the different FRC performance classes (**b**)

and EC2 [17], as illustrated in Fig. 8a and c. As earlier mentioned, MC10 [7] and EC2 [17] also consider a decreasing post-cracking branch in the constitutive tensile model for FRC class *c* and *d*, which is not always the case from a mechanical point-of-view (FRC *c* if $0.9 \leq f_{R3k}/f_{R1k} < 1.1$; FRC *d* if $1.1 \leq f_{R3k}/f_{R1k} < 1.3$). Therefore, the accuracy of those constitutive tensile models is not visualized in Fig. 8. But overall, the expected values at $CMOD_1$ and $CMOD_3$, by including the EC2 model at the different FRC classes, show the highest accuracy. Consequently, it is also evident from Figs. 7 and 8b, that especially the k'_c in Eq. (10) can be further optimized to obtain a higher accuracy. Nevertheless, it is worth noting that the newly developed constitutive models also show a quite accurate reproduction of the characteristic residual flexural tensile strength of the specimens. The maximal absolute error between the experimental and predicted characteristic residual strength at $CMOD_1$ and $CMOD_3$ is observed to be 0.18 MPa for FRC *a & b*; while for FRC *d*, it is 0.67 MPa.

Based on the above observations, it can be concluded that the new constitutive tensile models for FRC seem to be not only applicable for the investigated GFRC and PFRC mixtures, that were used to calibrate the models [18], but also for FRC mixtures with a broader range of fibres. However further optimization is needed at $CMOD_1$ and $CMOD_3$ for FRC *a & b* and FRC *d*.

5.2.3 Neutral axis location

Based on the measurements of the side LVDTs, glued on the surface (one side) of the specimens in [21], the neutral axis location of the investigated beam cross-section, i.e., that at midspan can be determined. Previous research [18] indicated that a linear deformation profile along the height of the beam cross-section can be assumed, and the neutral axis is located where the horizontal deformation is equal to zero. This assumption is valid for tests where time effects do not play a major role [21]. In Fig. 9, the solid line illustrates the (mean) neutral axis evolution for all the collected FRC mixtures in [21], based on the measurements of the LVDTs attached on one side surface of the beams specimens [21] and by the assumption of a linear deformation profile. The test data indicates that in the CMOD-range of [0.5–2.5 mm], the neutral axis of the midspan cross-section for all the investigated mixtures is located in the 125–150 mm range (measured from the bottom of the beam specimens), which is similar to that of the GFRC and PFRC mixtures

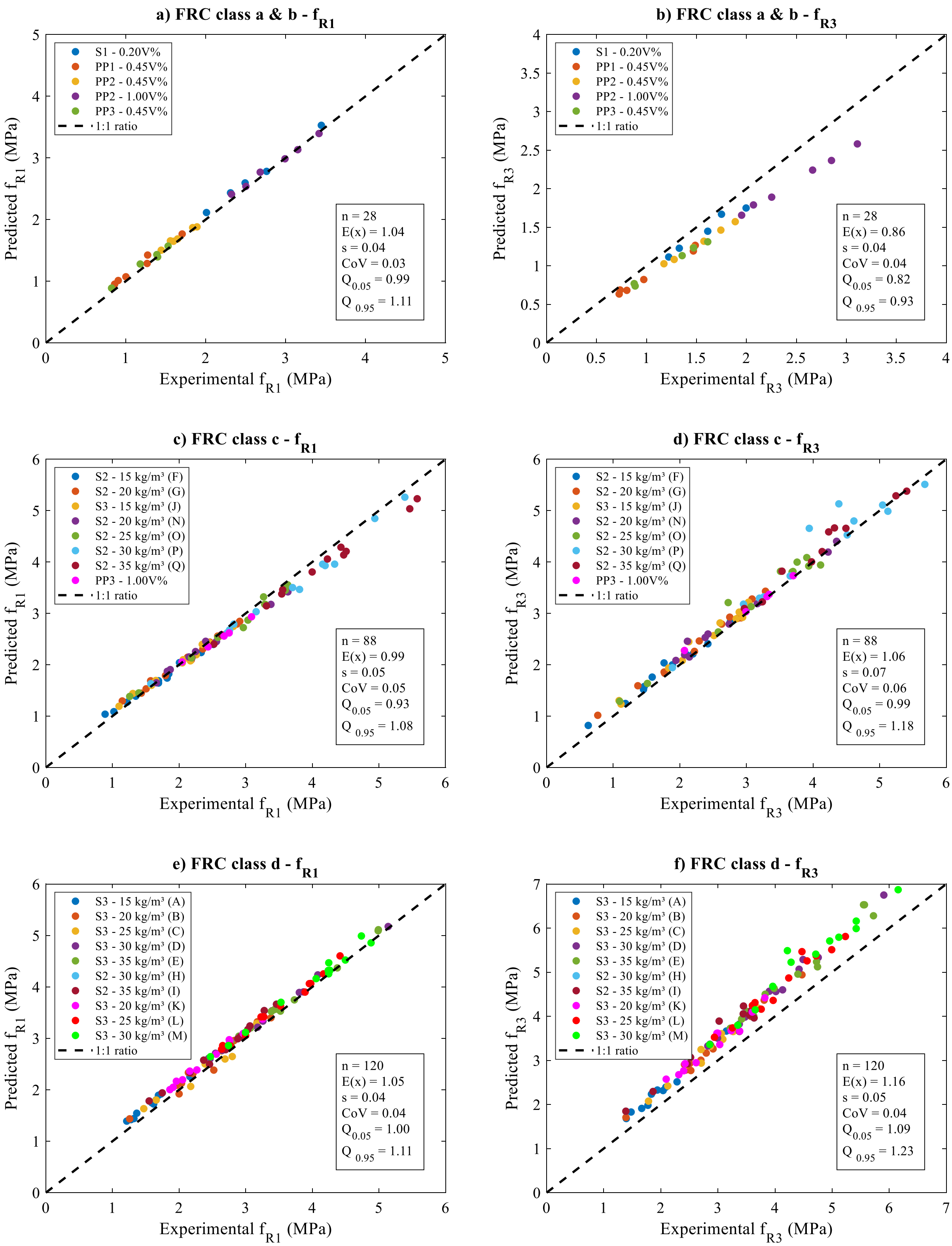
a) FRC class a & b - f_{R1}
S1 - 0.20V%
PP1 - 0.45V%
PP2 - 0.45V%
PP2 - 1.00V%
PP3 - 0.45V%
1:1 ratio
n = 28
E(x) = 1.04
s = 0.04
CoV = 0.03
$Q_{0.05}$ = 0.99
$Q_{0.95}$ = 1.11
Predicted f_{R1} (MPa)
Experimental f_{R1} (MPa)
b) FRC class a & b - f_{R3}
S1 - 0.20V%
PP1 - 0.45V%
PP2 - 0.45V%
PP2 - 1.00V%
PP3 - 0.45V%
1:1 ratio
n = 28
E(x) = 0.86
s = 0.04
CoV = 0.04
$Q_{0.05}$ = 0.82
$Q_{0.95}$ = 0.93
Predicted f_{R3} (MPa)
Experimental f_{R3} (MPa)
c) FRC class c - f_{R1}
S2 - 15 kg/m³ (F)
S2 - 20 kg/m³ (G)
S3 - 15 kg/m³ (J)
S2 - 20 kg/m³ (N)
S2 - 25 kg/m³ (O)
S2 - 30 kg/m³ (P)
S2 - 35 kg/m³ (Q)
PP3 - 1.00V%
1:1 ratio
n = 88
E(x) = 0.99
s = 0.05
CoV = 0.05
$Q_{0.05}$ = 0.93
$Q_{0.95}$ = 1.08
Predicted f_{R1} (MPa)
Experimental f_{R1} (MPa)
d) FRC class c - f_{R3}
S2 - 15 kg/m³ (F)
S2 - 20 kg/m³ (G)
S3 - 15 kg/m³ (J)
S2 - 20 kg/m³ (N)
S2 - 25 kg/m³ (O)
S2 - 30 kg/m³ (P)
S2 - 35 kg/m³ (Q)
PP3 - 1.00V%
1:1 ratio
n = 88
E(x) = 1.06
s = 0.07
CoV = 0.06
$Q_{0.05}$ = 0.99
$Q_{0.95}$ = 1.18
Predicted f_{R3} (MPa)
Experimental f_{R3} (MPa)
e) FRC class d - f_{R1}
S3 - 15 kg/m³ (A)
S3 - 20 kg/m³ (B)
S3 - 25 kg/m³ (C)
S3 - 30 kg/m³ (D)
S3 - 35 kg/m³ (E)
S2 - 30 kg/m³ (H)
S2 - 35 kg/m³ (I)
S3 - 20 kg/m³ (K)
S3 - 25 kg/m³ (L)
S3 - 30 kg/m³ (M)
1:1 ratio
n = 120
E(x) = 1.05
s = 0.04
CoV = 0.04
$Q_{0.05}$ = 1.00
$Q_{0.95}$ = 1.11
Predicted f_{R1} (MPa)
Experimental f_{R1} (MPa)
f) FRC class d - f_{R3}
S3 - 15 kg/m³ (A)
S3 - 20 kg/m³ (B)
S3 - 25 kg/m³ (C)
S3 - 30 kg/m³ (D)
S3 - 35 kg/m³ (E)
S2 - 30 kg/m³ (H)
S2 - 35 kg/m³ (I)
S3 - 20 kg/m³ (K)
S3 - 25 kg/m³ (L)
S3 - 30 kg/m³ (M)
1:1 ratio
n = 120
E(x) = 1.16
s = 0.05
CoV = 0.04
$Q_{0.05}$ = 1.09
$Q_{0.95}$ = 1.23
Predicted f_{R3} (MPa)
Experimental f_{R3} (MPa)

◂**Fig. 7** Ratio of the predicted and experimental f_{R1} or f_{R3}-values by use of the new constitutive tensile models for FRC class *a* & *b* (**a–b**), FRC class *c* (**c–d**), FRC class *d* (**e–f**)

which were used to develop the new constitutive tensile models [18].

Figure 9 also presents the predicted neutral axis evolution in the beam cross-section at mid-span (dashed line), based on the measured mean stress-CMOD curve and with the new constitutive tensile models. The predicted neutral axis evolution with the new model for FRC class *a* and *b* is found to be very close to the measured one. Three FRC mixtures, namely PP1-0.45 V%, PP2-0.45 V%, and PP2-1.00 V%, exhibit a lower measured Y_{NA}-location than the predicted one. As such, this is not only related to the higher fibre content (1.00 V%), but also to the increased fibre length of the PP fibres (55 and 54 mm) in comparison to the glass fibres (length: 43 mm; fibre content: 0.50 and 0.75 V%) that were used to develop the new model. The other FRC mixtures with performance class *a* and *b* show the opposite behaviour, that is, a lower predicted neutral axis location than the measured one. This is apparently related to the lower fibre content or the smaller fibre length, compared with the glass fibres, used in the development of the models [18]. A similar conclusion can be made for the FRC mixture of class *c*, see Fig. 9c). The small difference between the predicted and measured Y_{NA}-values only slightly influence the predicted stress–CMOD curve.

Figure 10 presents the predicted Y_{NA}-evolution of all the specimens of a specific FRC class. As revealed from the figure, a lower Y_{NA}-value is found for a higher FRC class. Obviously, this is reasonable because of the improved post-cracking performance with the increase of the FRC performance class. However, the median of the predicted Y_{NA}-values at 0.5 mm CMOD only decreases from 138.2 to 135.7 mm when the FRC performance class increases from *a* & *b* to *d*. At $CMOD_3$, the difference between that value for different FRC classes becomes even smaller.

As mentioned in Sect. 1, the model in MC10 [7] assumes a fixed value for the k'_a-parameter, which is 0.45. The assumption of that value can satisfy the equilibrium condition for bending moment, but not (necessarily) for the horizontal force. Therefore, Vrijdaghs et al. [21] indicated that the use of the MC10 model consistently overestimates the height of the compressive zone. However, although the scattering of the compression zone height, the new constitutive models show a good one-to-one relationship between the experimental and predicted compressive zone height (x), as plotted in Fig. 11.

In addition, it is very interesting to find that the collected 236 monotonic test data shows a strong correlation between the experimental f_{R1}-values, as well as the f_{R3}-values, and the predicted compression

Table 3 Statistical parameters for evaluating the predictive accuracy of different models

	Evaluation of $f_{R1,pred}/f_{R1,exp}$					Evaluation of $f_{R3,pred}/f_{R3,exp}$				
	$E(X)$	s	CoV	$Q_{0.05}$	$Q_{0.95}$	$E(X)$	s	CoV	$Q_{0.05}$	$Q_{0.95}$
FRC class *a*, *b*										
MC10	1.35	0.06	0.04	1.26	1.43	1.13	0.18	0.16	0.79	1.41
EC2	1.11	0.05	0.04	1.05	1.19	1.05	0.08	0.08	0.96	1.20
New model	1.04	0.04	0.03	0.99	1.11	0.86	0.04	0.04,	0.82	0.93
FRC class *c*										
MC10	1.25	0.05	0.04	1.19	1.37	1.05	0.07	0.07	0.97	1.18
EC2	1.02	0.05	0.05	0.96	1.14	0.95	0.05	0.05	0.90	1.03
New model	0.99	0.05	0.05	0.93	1.08	1.06	0.07	0.06	0.99	1.18
FRC class *d*										
MC10	1.23	0.04	0.03	1.18	1.30	0.92	0.04	0.04	0.89	0.97
EC2	1.00	0.05	0.05	0.95	1.08	1.01	0.05	0.05	0.95	1.12
New model	1.05	0.04	0.04	1.00	1.11	1.16	0.05	0.04	1.09	1.23

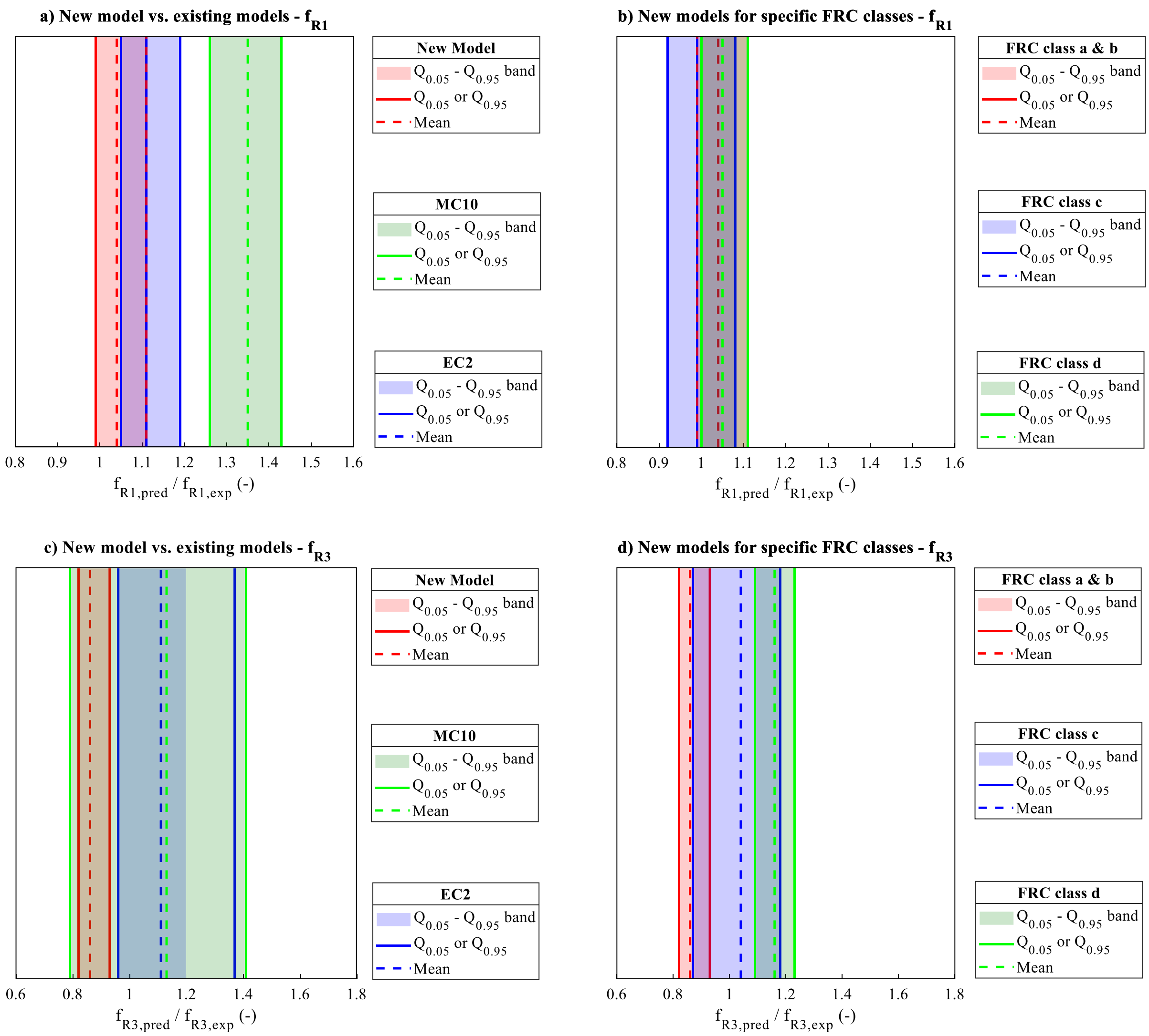

Fig. 8 Comparison of the accuracy of the new constitutive model and the model in MC10 [1] and EC2 [17] at $CMOD_1$ and $CMOD_3$ for FRC class *a* & *b* (a and c), and the accuracy of the new constitutive tensile model for a specific FRC performance class at $CMOD_1$ and $CMOD_3$ (b and d)

zone height of the beam midspan cross-section at the corresponding CMOD level, as indicated in Fig. 12. The empirical relations derived through regression analysis of the data are presented in Eqs. (27) and (28), respectively. As can be observed from Fig. 12, these two equations are valid irrespective of the FRC class. An increase of the f_{R1}- or f_{R3}-values leads to an increase of the compression zone height of the beam cross-section at midspan, and vice versa.

$$x = 4.3 f_{R3}^{2/5} \text{ for } f_{R3} \in [0.6\text{ MPa}, 6.8\text{ MPa}] \tag{27}$$

$$x = 10 f_{R1}^{1/3} \text{ for } f_{R1} \in [0.8\text{ MPa}, 5.6\text{ MPa}] \tag{28}$$

where x = height of the compression zone (mm); f_{R1} and f_{R3} = residual tensile strength (MPa) at 0.5 and 2.5 mm CMOD, respectively.

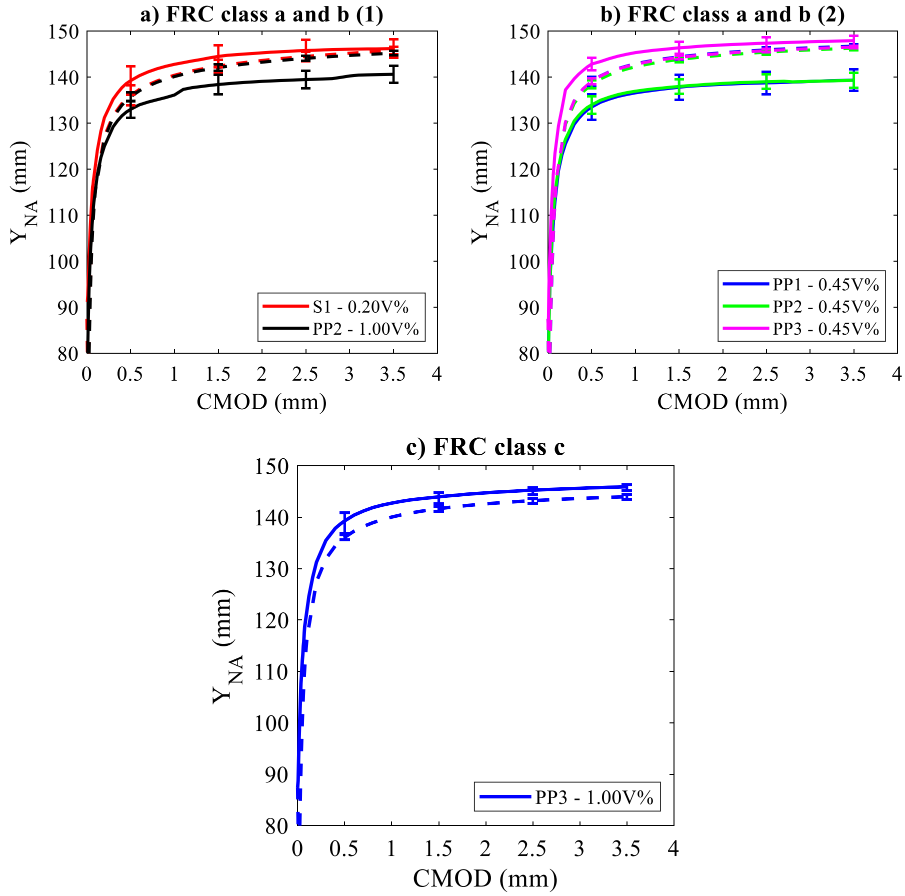

Fig. 9 Comparison of the mean tested (solid line) and predicted Y_{NA}-evolution with the new constitutive tensile models (dashed line)

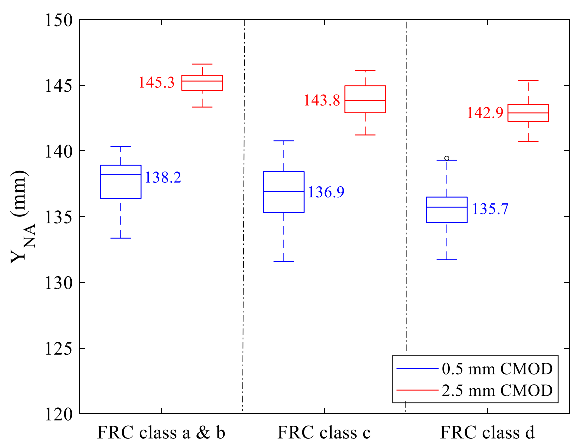

Fig. 10 Predicted neutral axis location at 0.5 and 2.5 mm CMOD for all investigated FRC mixtures with the new constitutive tensile models for different FRC classes

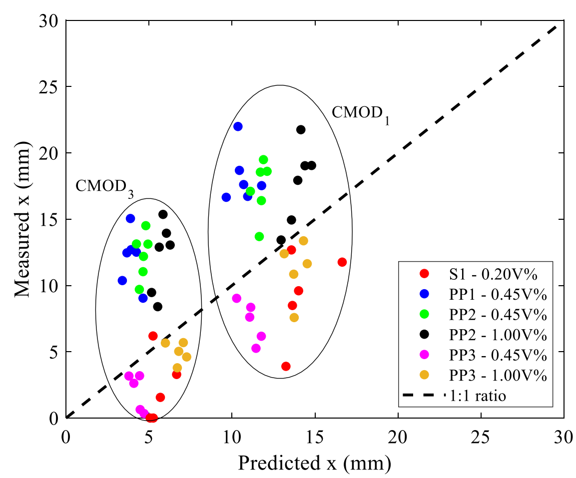

Fig. 11 Ratio of the measured and predicted compressive zone height according to the new constitutive tensile models

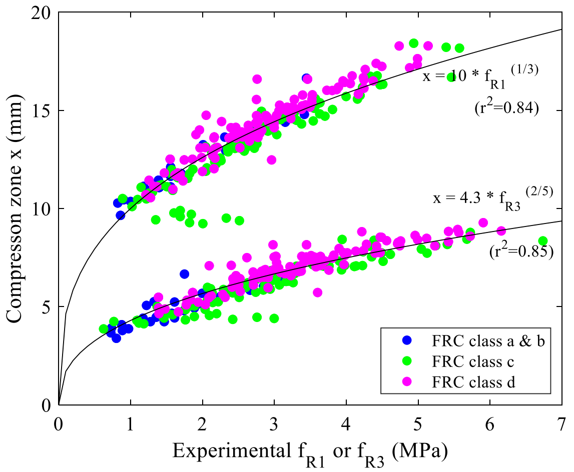

Fig. 12 Relation between the experimental f_{R1} or f_{R3}-values and the predicted compression zone height x for different FRC classes

6 Conclusions

This paper presents a verification of the three newly developed constitutive tensile models [18] for FRC, as well as the model for predicting the residual flexural tensile strength of FRC mixtures proposed by Oettel et al. [14]. This was done by using the test data in [21] and that of the international company Bekaert. The whole database consists of a total of 236 notched FRC beams with three types of macro steel fibres and three types of macro PP fibres. Based on the research results, the following conclusions can be drawn:

- The proposed model of Oettel et al. [14] underestimates the residual flexural tensile strength values at $CMOD_1$ and $CMOD_3$ for FRC mixtures with 4D Dramix fibres. This is believed to be related to the underestimation of the χ-parameter in Oettel's approach if a double-bended anchorage system is used. Therefore, the χ-parameter is optimized for the specific 4D Dramix fibres. This is done by the least square method. The optimized χ-value is 0.44, and the mean value of the ratio of the predicted f_{R1} and f_{R3}-values to their measured counterpart is 1.13 and 0.97, if this specific χ-value is used. However, further research is required to clarify if the underestimation, by using Oettel's model, is also observed for other steel fibres or just for this specific anchorage system.
- The magnitude of the parameter ε_p, which represents the strain at peak stress in the constitutive tensile model for FRC in MC10 [7], has a large influence on the predicted flexural tensile strength of the FRC specimens. The numerical results indicate that when that parameter is assumed as 0.010%, the predicted flexural tensile strength is closer to the measured value, in comparison to that with $\varepsilon_P = 0.015\%$. (as recommended in MC10 [7]). Similar results were also found in [18].
- The new constitutive tensile model for FRC class *a & b*, FRC class *c*, and FRC *d* provide quite accurate predictions of the residual tensile strength at $CMOD_1$. The smallest $f_{R1,pred}/f_{R1,exp}$ ratio is 0.99 for FRC *c*, while FRC class *a & b* and FRC class *d* indicate a ratio of 1.04 and 1.05, respectively. Next to this, an increased deviation at $CMOD_1$ is observed when the model of the future EC2 (next version) [17] and MC10 [7] for FRC class *a & b* and FRC class *c* is used.
- The new constitutive tensile model for FRC class *c* indicates a high accuracy not only at $CMOD_1$ but also at $CMOD_3$. The $f_{R3,pred}/f_{R3,exp}$ ratio is found to be 1.06. Nevertheless, although there is a narrow $Q_{0.05}$ and $Q_{0.95}$ range at $CMOD_3$ for the different FRC classes, there is a scope to further optimize the newly developed FRC *a & b* and FRC class *d* model at $CMOD_3$.
- The use of the new constitutive tensile models for FRC leads to a small difference between the predicted and measured neutral axis location of the beam cross-section at midspan. In addition, a good one-to-one relation between the measured and predicted compression zone height of the midspan cross-section is found for all the FRC specimens.
- There is a strong correlation between the experimental f_{R1}-values, as well as the f_{R3}-values, and the predicted compression zone height of the midspan cross-section with the newly developed models for FRC, as shown in Eqs. (27) and (28), respectively. An increase of the f_{R1}- or f_{R3}-values leads to an increase of the compression zone height of the beam cross-section at midspan, and vice versa.

Declarations

Conflict of interest The authors declare that they have no known competing financial interests or personal relationships that could have appeared to influence the work reported in this paper.

References

1. Fike R, Kodur V (2011) Enhancing the fire resistance of composite floor assemblies through the use of steel fiber reinforced concrete. Eng Struct 33(10):2870–2878. https://doi.org/10.1016/j.engstruct.2011.06.011
2. Zamri NF, Mohamed RN, Awalluddin D, Abdullah R (2022) Experimental evaluation on punching shear resistance of steel fibre reinforced self-compacting concrete flat slabs. J Build Eng 52:104441. https://doi.org/10.1016/j.jobe.2022.104441
3. Nogales A, de la Fuente A (2021) Numerical-aided flexural-based design of fibre reinforced concrete column-supported flat slabs. Eng Struct 232:111745. https://doi.org/10.1016/j.engstruct.2020.111745
4. Caratelli A, Meda A, Rinaldi Z, Romualdi P (2011) Structural behaviour of precast tunnel segments in fiber reinforced concrete. Tunn Undergr Space Technol 26(2):284–291. https://doi.org/10.1016/j.tust.2010.10.003
5. Carlos TB, Rodrigues JPC, de Lima RCA, Dhima D (2018) Experimental analysis on flexural behaviour of RC beams strengthened with CFRP laminates and under fire conditions. Compos Struct 189:516–528. https://doi.org/10.1016/j.compstruct.2018.01.094
6. Blanco A, Pujadas P, De La Fuente A, Cavalaro S, Aguado A (2013) Application of constitutive models in European codes to RC-FRC. Constr Build Mater 40:246–259. https://doi.org/10.1016/j.conbuildmat.2012.09.096
7. Special Activity Group 5, fib Model Code 2010, no. September. Wilhelm Ernst & Sohn, Berlin. https://doi.org/10.1002/9783433604090.ch6.
8. Tiberti G, Germano F, Antonio M, Plizzari GA (2018) An overview of the flexural post-cracking behavior of steel fiber reinforced concrete. Struct Concr 19(3):695–718
9. Conforti A, Zerbino R, Plizzari GA (2019) Influence of steel, glass and polymer fibers on the cracking behavior of reinforced concrete beams under flexure. Struct Concr 20(1):133–143. https://doi.org/10.1002/suco.201800079
10. Infrastructuur in het Leefmilieu, "Dramix Guideline [final draft] Design of concrete structures - Steel wire fibre reinforced concrete structures with or without ordinary reinforcement.," 1995.
11. Falkner H, Teutsch M (1993) Untersuchung des Biegetragverhaltens von Stahlfaserbetonbalken unter Variation der Faserart. iBMBForschungsbericht, Braunsweig, Germany: Institut für Baustoffe, Massivbau und Brandschutz.
12. Falkner H, Teutsch M, Klinkert H (1999) "Leistungsklassen von Stahlfaserbeton," Braunsweig, Germany: Institut für Baustoffe, Massivbau und Brandschutz.
13. Teutsch M (1993) Bemessungsgrundsätze für Bauteile aus Stahlfaserbeton Hochtief-Kolloquium 'Entwicklung und Einsatz von Stahlfaserbeton.' Frankfurt, Germany
14. Oettel V, Schulz M, Haist M (2022) Empirical approach for the residual flexural tensile strength of steel fiber-reinforced concrete based on notched three-point bending tests. Struct Concr 23(2):993–1004. https://doi.org/10.1002/suco.202100565
15. CEN, "EN 14651: Tet method for metallic fibre concrete—measuring the flexural tensile strength (limit of proportionality (LOP), residual)," Brussels (2005).
16. di Prisco M, Colombo M, Dozio D (2013) Fibre-reinforced concrete in fib Model Code 2010: principles, models and test validation. Struct Concr 14(4):342–361. https://doi.org/10.1002/suco.201300021
17. di Prisco M, Kanstad T, Plizzari G, Minelli F, Haus A (2022) Eurocode 2—Annex L—European Harmonized Standard for Steel Fibre Reinforced Concrete," pp. 539–551. https://doi.org/10.1007/978-3-030-83719-8_47.
18. Vandevyvere B (2022) Post-cracking behaviour of fibre reinforced recycled concrete. PhD thesis, KU Leuven.
19. Vandevyvere B, Vandewalle L, Li J (2023) Numerically optimized post-cracking branch of the constitutive tensile model for fiber-reinforced concrete with natural and recycled aggregates. Struct Concr. https://doi.org/10.1002/suco.202200574
20. Vandevyvere B, Vandewalle L, Li J (2022) Improved simplified constitutive tensile model for fibre reinforced concrete. J Federat Struct Concrete. 24(4):4624–44. https://doi.org/10.1002/suco.2022003594644VANDEVYVEREETAL
21. Vrijdaghs R, Van Itterbeeck P, De Smedt M, Vandewalle L (2021) Experimental study into the location of the neutral axis in fiber-reinforced concrete prisms. Struct Concr 22(1):285–297. https://doi.org/10.1002/suco.201900397
22. Abdallah S, Fan M, Rees DWA (2016) Analysis and modelling of mechanical anchorage of 4D/5D hooked end steel fibres. Mater Des 112:539–552. https://doi.org/10.1016/j.matdes.2016.09.107.
23. Abdallah S, Fan M (2017) Anchorage mechanisms of novel geometrical hooked-end steel fibres. Mater Struct 50(2):139. https://doi.org/10.1617/s11527-016-0991-5
24. Bureau voor Normalisatie, "NBN EN 1990+A1: Eurocode - Grondslagen van het constructief ontwerp," (2015).
25. Bureau voor Normalisatie, "NBN EN 12390–3: Beproeving van verhard beton - Deel 3 : Druksterkte van proefstukken (+ AC:2011),(2009).
26. Dupont D, Vandewalle L (2005) Distribution of steel fibres in rectangular sections. Cem Concr Compos 27(3):391–398. https://doi.org/10.1016/j.cemconcomp.2004.03.005
27. Kooiman A (2000) Modelling steel fibre reinforced concrete for structural design. PhD thesis, TU Delft.
28. Grünewald S (2004) Performance-based design of self-compacting fibre reinforced concrete. PhD thesis, TU Delft.
29. Soetens T, Matthys S (2014) Different methods to model the post-cracking behaviour of hooked-end steel fibre reinforced concrete. Constr Build Mater 73:458–471. https://doi.org/10.1016/j.conbuildmat.2014.09.093
30. Vrijdaghs R, di Prisco M, Vandewalle L (2021) Sectional analysis of the flexural creep of cracked fiber reinforced concrete. Struct Concr 22(3):1817–1830. https://doi.org/10.1002/suco.202000559